Directional wave measurements from three wave sensors during the FETCH experiment

Heidi Pettersson, Hans C. Graber, Danièle Hauser, Céline Gwenaëlle Quentin, Kimmo K. Kahma, William M. Drennan, Mark A. Donelan

Directional wave measurements from three wave sensors during the FETCH experiment

Heidi Pettersson,[1] Hans C. Graber,[2] Danièle Hauser,[3] Céline Quentin,[3] Kimmo K. Kahma,[1] William M. Drennan,[2] and Mark A. Donelan[2]

Received 9 October 2001; revised 5 March 2002; accepted 11 March 2002; published 11 March 2003.

[1] During the Flux, Etat de la mer et Télédéction en Condition de fetcH variable (FETCH) experiment, directional wave measurements were made by an airborne radar RESSAC and by two moored buoys, an Air–Sea Interaction Spar (ASIS) and a Directional Waverider. In order to define the performance and compatibility of these wave sensors with different measuring principles, a comparison of the directional measurements in a variety of meteorological conditions during the experiment is presented in this paper. It was found that within the limits of their operational ranges, the sensors agreed on the one-dimensional spectrum and the basic parameters derived from it—significant wave height and peak frequency. The sensors reported the directional features of the wave field and the mean direction consistently, but in some cases the two buoys disagreed on the directional width of the spectrum. Most of these cases were associated with a single swell-dominated event. *INDEX TERMS:* 4560 Oceanography: Physical: Surface waves and tides (1255); 4594 Oceanography: Physical: Instruments and techniques; 4546 Oceanography: Physical: Nearshore processes; 4223 Oceanography: General: Descriptive and regional oceanography; *KEYWORDS:* wave sensor, directional spectrum, FETCH, comparison

Citation: Pettersson, H., H. C. Graber, D. Hauser, C. Quentin, K. K. Kahma, W. M. Drennan, and M. A. Donelan, Directional wave measurements from three wave sensors during the FETCH experiment, *J. Geophys. Res.*, *108*(C3), 8061, doi:10.1029/2001JC001164, 2003.

1. Introduction

[2] Over the past 20 years, many new sensors have been developed to measure directional properties of ocean waves. Traditional sensors, including buoys and arrays of wave height sensors, are well suited for continuous time series measurements at fixed, usually coastal, locations. Newer techniques using remote sensing take advantage of the greatly enhanced spatial coverage offered by satellites or aircraft. Among the present sensors only HF (high frequency) radar can provide both temporal and spatial coverage. In situ and remotely sensed measurements are complementary in that the former provide good temporal resolution at a few locations, while the latter provide superior spatial coverage at selected (short or infrequent) time periods. Often experimental goals are best achieved through a combination of in situ and remotely sensed data, with model output used to fill in the gaps. Consequently, there is considerable interest in developing the ability to integrate data from different sources.

[3] There have been a number of recent papers dedicated to the intercomparison of different directional wave sensors. These include *Allender et al.* [1989], who compare seven wave buoys deployed side-by-side at a site in the North Sea, *O'Reilly et al.* [1996], who compare Directional Waverider (DWR) and heave-pitch-roll buoys against a pressure array, and *Wyatt et al.* [1999], who compare a DWR with an HF radar. In addition, the volume edited by *Beal* [1991] contains many related papers from the LEWEX experiment, along with comparisons between measurements and models.

[4] While the different wave sensors in general agree quite well on the one-dimensional spectrum and the basic parameters derived from it, the results concerning the directional spectrum have not been as satisfactory. Also as the operational principles of many of the sensors differ, as do the methods of analysis, consensus has not yet been reached on a clear set of parameters for comparing directional wave data. *Krogstad et al.* [1999] recently addressed this issue, and identified five "most central" sea state parameters: the significant wave height, H_s, the mean and spectral peak periods, the mean wave direction and the directional spreading, the latter two being functions of frequency. *Krogstad et al.* [1999] also show the importance of estimating the sampling variability associated with the data being compared: significant differences between instruments will be indicated by variability greater than the expected sampling variability.

[5] In this paper we compare three directional wave sensors that were operated during the FETCH experiment

[1]Finnish Institute of Marine Research, Helsinki, Finland.
[2]Rosenstiel School of Marine and Atmospheric Science, University of Miami, Miami, Florida, USA.
[3]Centre d'Etude des Environnements Terrestres et Planétaires, Vélizy, France.

0148-0227/03/2001JC001164

in 1998. One of the wave sensors is an airborne radar (RESSAC) of Centre d'Etude des Environnements Terrestres et Planétaires [*Hauser et al.*, 1992]. The two others are moored buoys, of which one is an Air–Sea Interaction Spar (ASIS) developed by Rosenstiel School of Marine and Atmospheric Science and Woods Hole Oceanographic Institution [*Graber et al.*, 2000] and the other is a commercial buoy, a Directional Waverider produced by Datawell b.v. The comparison is done in two parts. We compare first the two buoys which were moored side by side for a one week period. We then compare the airborne radar to the two buoys during overflights made by the aircraft.

1.1. FETCH Experiment

[6] The experimental area of FETCH (Flux, Etat de la mer et Télédétection en Condition de fetcH variable), an extensive experiment for studies of air–sea interactions and fetch limited wave growth in high wind conditions [*Hauser et al.*, 2003], was the Gulf of Lion in the northwestern Mediterranean Sea (Figure 1). During the experiment a ship and several buoys were operated for in situ measurements while instrumented aircrafts and satellites provided remote sensing observations. The time period of the experiment, from 12 March to 16 April 1998, was chosen to coincide with the expected period of high offshore winds: Mistrals from the north, and Tramontane winds from the northwest.

[7] During the first part of the experiment the ASIS and DWR buoys were deployed at 42°58′56″N, 04°15′11″E, roughly 60 km from the shore (point B in Figure 1), for a side-by-side intercomparison. The distance between the buoys was approximately 2 km and the depth at the mooring site 100 m. DWR was moored on 16 March and ASIS a couple of days later on 18 March. On 25 March, DWR was recovered and redeployed at 43°09′34″N, 04°06′15″E, 25 km north–northwest from ASIS (point B′ in Figure 1). The water depth at this location was 90 m. The radar RESSAC was installed on board the Merlin-IV aircraft of the French Meteorological Office (Météo France). Wave measurements using RESSAC were made along flight tracks which passed over the locations of the moored buoys. Some of the RESSAC tracks were also simultaneous with overpasses from the satellite TOPEX-Poseidon.

[8] The meteorological data used in this study were measured on ASIS and on R/V *l'Atalante*. Both platforms employed sonic anemometers, at heights 7 m and 17 m respectively. Details of the ASIS meteorological sensors are given by *Drennan et al.* [2003a]; see *Dupuis et al.* [2003] for information on R/V *l'Atalante* systems. The time series of wind speed, wind direction and significant wave height as measured by ASIS are plotted in Figures 2 and 3. During the first part of the experiment when the two moored buoys were deployed side by side, the meteorology was dominated by two Mistral events on 19–21 and on 24 March (Figure 2). The meteorology during the remaining period of the experiment was more complicated with inhomogeneous wind fields and frontal discontinuities in the western Mediterranean Sea (Figure 3). The larger scale meteorological conditions are provided by the atmospheric circulation model Aladin, which is a regional adaption of the global atmospheric model of Météo-France. The model is run twice a day at 0000 and 1200 UTC. Aladin uses a 10 km grid on the western Mediterranean Sea, and provides atmospheric variables every three hours.

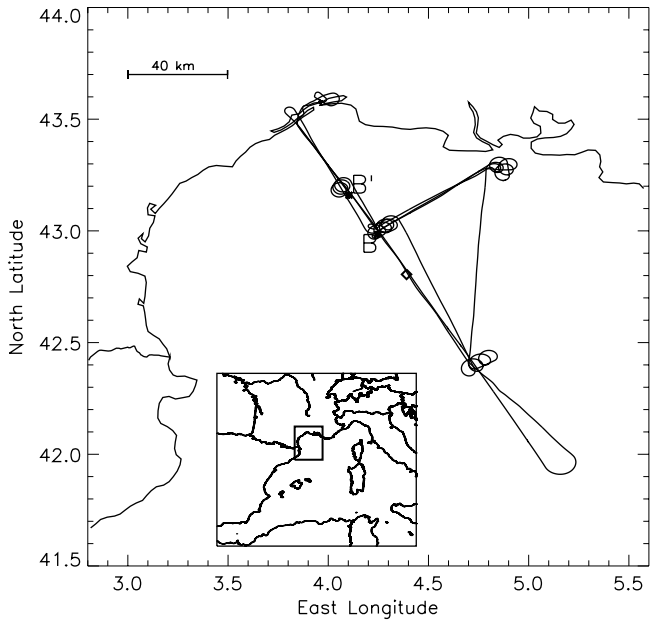

Figure 1. Geographic map of the FETCH experiment. Point B (42.98°N, 4.25°E) is the location of the ASIS buoy from 18 March to 9 April. DWR was also at this location from 16 March to 25 March. Point B′ (43.16°N, 4.10°E) is the location of DWR after 25 March. The solid line shows, for the case of 3 April, the trajectory of the Merlin-IV aircraft with RESSAC on board. Data in the wave mode of RESSAC were obtained along the northwest–southeast part of the trajectory. The diamond shows the location of R/V *l'Atalante* during the intercomparison period on 3 April.

2. Wave Sensors

2.1. Real-Aperture Radar RESSAC

[9] The real-aperture airborne radar RESSAC (Radar pour l'Etude du Spectre de Surface par Analyze Circulaire) is a C-band radar with a scanning beam antenna. During FETCH, RESSAC was used in three different modes: the wave mode to acquire directional wave spectra, the scatterometer mode for wind and flux measurements, and the low altitude mode to obtain the normalized radar cross-section. The basic processing of the wave mode data was done following *Hauser et al.* [1992]. The principle of measurement is based on the measurement of the modulation of the radar backscatter coefficient due to the slopes of longer waves. A large antenna (14° elevation × 3.4° azimuth) looking at a mean incidence angle of 14° from a flight altitude of about 6000 m gives a footprint size of 1500 m × 400 m. With this configuration the backscatter modulation is dominated by the tilt effect so that its density spectrum is linearly related to the slope spectrum of the waves [*Jackson and Walton*, 1985; *Jackson et al.*, 1985; *Hauser et al.*, 1992]. The antenna scans at a rate of

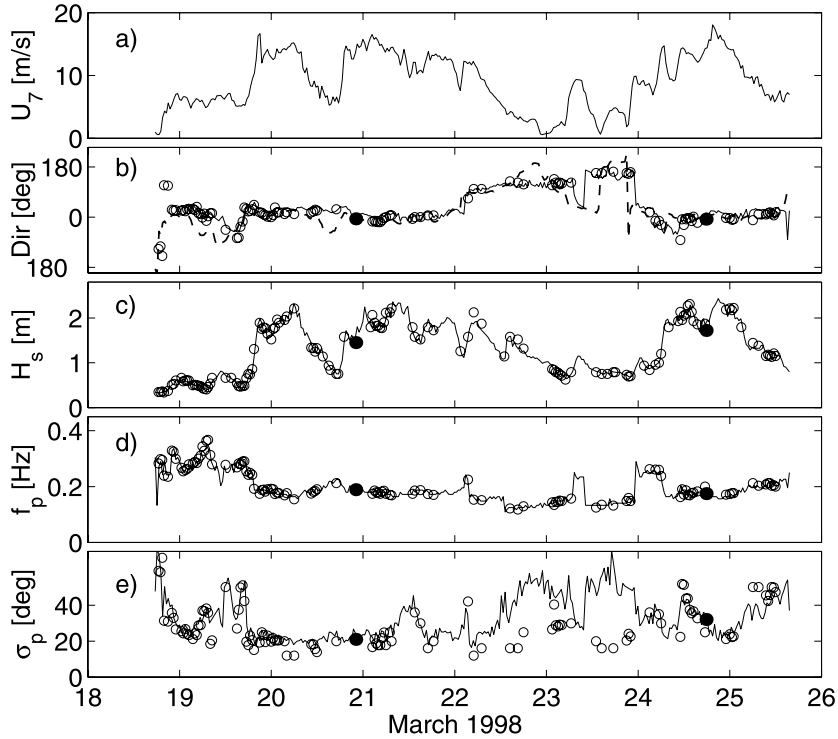

Figure 2. Conditions during the period when the two wave buoys were deployed at the same location B. ASIS, DWR and RESSAC data are indicated by a solid line, ○ and ● (20 and 24 March), respectively. Panel a) indicates the 7 m wind speed. Panel b) shows the peak wave directions. For reference, the wind direction from ASIS is also shown (dashed line). The directions indicated are those the wind or waves are arriving from. Panel c) indicates significant wave height. Panel d) shows peak wave frequency. Panel e) indicates the directional spreading at the peak frequency.

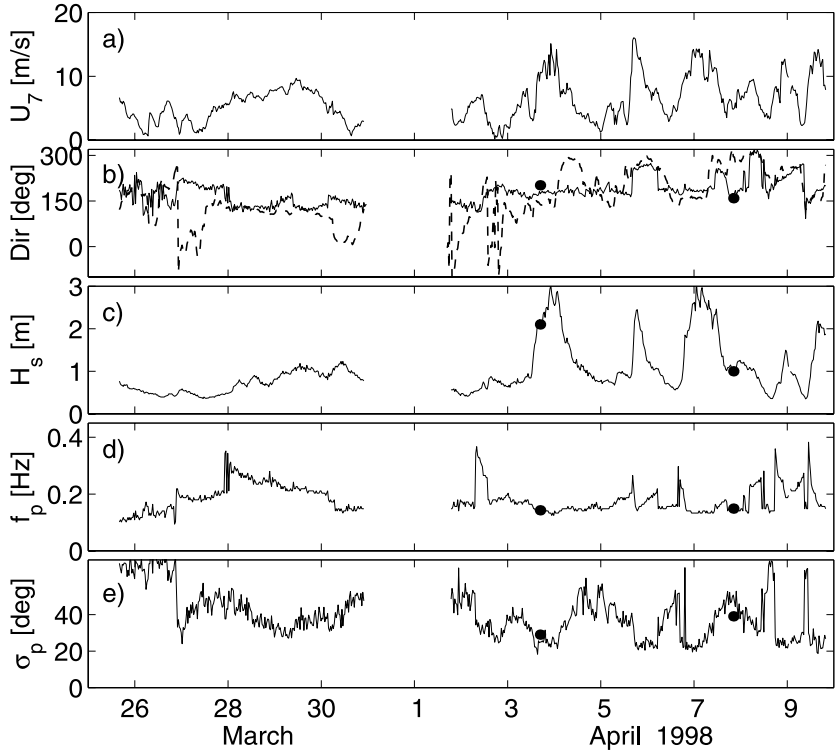

Figure 3. Conditions during the second part of the experiment as reported by ASIS at location B. Panel a) shows the 7 m wind speed. Panel b) shows the direction the peak waves (solid line) and wind (dashed line) are arriving from. Panel c) shows the significant wave height, panel d) the peak wave frequency and panel e) the directional spreading at the peak frequency. The RESSAC data (3 and 7 April) are indicated by ●.

three rotations per minute in the azimuth to cover all the directions giving a rather direct estimate of the two-dimensional spectrum.

[10] The directional spectrum is calculated at 64 wave numbers which, using the dispersion relation for gravity waves in deep water, corresponds to a frequency range of 0.05 to 0.25 Hz. The energy density is averaged over 15° in direction and over 5 successive scans of the antenna. The time interval for the final spectrum is thus 1 min 40 s corresponding to a spatial extension of about 10 km along the aircraft track. The wavelength resolution depends on the wavelength itself, being typically about 10% of it. RESSAC provides a reliable estimate of two-dimensional wave spectrum for significant wave heights over 1 m and wavelengths longer than 30–40 m. These limitations are due to speckle noise and to the principle of measurement (assumption of linearity), respectively. As the radar measurements are related to the tilt of the waves which are nearly symmetric with respect to the crests, the two-dimensional spectrum has a 180° ambiguity. For a detailed description of the radar and data processing, see *Hauser et al.* [1992].

[11] All the spectra measured during FETCH had a spurious background spectrum which had a high energy level at lower frequencies with decreasing trend toward higher frequencies. This background level was removed after estimating it by analyzing the radar signal in the absence of the waves. Furthermore there was an underestimation of the energy density which was corrected on the basis of coincident TOPEX-Poseidon satellite measurements of significant wave heights [*Quentin and Hauser*, 1999]. Merlin-IV made 11 flights during FETCH, and directional spectra were obtained from 7 of them.

2.2. Air–Sea Interaction Spar, ASIS

[12] The ASIS buoy was developed as a platform from which to make high resolution measurements near the air–sea interface [*Graber et al.*, 2000]. The buoy is a multispar design, employing a pentagonal cage of slender cylinders (22 cm diameter by 3.5 m long) which are joined to a central spar element approximately 3 m below the mean surface. This central spar is terminated with a drag plate roughly 7 m below the surface. The overall dimensions of ASIS buoy are 9 m long by 1 m radius (at the surface). A sonic anemometer, measuring the wind vector, along with temperature and humidity sensors were mounted on a 4 m high mast. During FETCH, the ASIS buoy was deployed in a moored configuration, tethered to a secondary buoy to isolate additional downward forces.

[13] The local surface elevation was measured by an array of 3.3 m long $\times$ 0.9 mm diameter capacitance wave gauges which were distributed in and around the ASIS cage. Here we use the data from an array of 6 gauges positioned as follows: five were mounted along the outer perimeter of the buoy, in a pentagon of 92.7 cm radius, and a sixth was mounted at the center of the buoy. This 6-element centered pentagon array is able to resolve waves of lengths greater than about 2 m. During the first half of the experiment (March 1998) one of the wave gauges at the outer perimeter was broken. All six staffs were operational during the second half of the experiment in April. The wave staffs were calibrated at RSMAS prior to deployment in the field.

[14] In order to make wave array measurements from a nonstationary platform such as ASIS, the motion of the platform must be accurately recorded. The ASIS buoy is equipped with a ''strapped down'' motion package located, along with the data acquisition system, in a watertight housing at the base of the buoy. The three orthogonal components of linear acceleration are measured with Columbia Research Laboratory accelerometers, while the three components of rotational motion are measured with solid state angular rate gyros (Systron Donner). Pre- and postfield calibrations of the ASIS motion sensors were carried out at the National Water Research Institute (NWRI), Burlington, Canada. Since the performance of the rate gyros declines at low frequencies, low frequency (<0.04 Hz) angular motion was determined using either a compass (for yaw) or the tilt angles derived from the appropriate linear accelerometers (for pitch and roll). The high and low frequency angular motions are combined using complementary filtering. Details of the algorithms are given by *Drennan et al.* [1994, 1998]. All ASIS data were sampled at 12 Hz, and processed in blocks of 28.5 min.

2.3. Directional Waverider

[15] Directional Waverider, a 90 cm diameter sphere, is a surface following buoy that measures the three components of linear acceleration. The vertical acceleration (heave), along with pitch and roll, are measured using a Hippy40, a stabilized platform. The two horizontal components of acceleration are measured with accelerometers fixed to the buoy hull, which are converted on-board to axes aligned with north and west using the measured angles, and a three axis fluxgate compass. These data are double integrated to yield displacements, and further processed on board using Fourier analysis, following *Longuet-Higgins et al.* [1963]. Spectra are calculated at 64 frequency bins from 1600 s of data. Each half hour, the following data were transmitted via HF radio to R/V *l'Atalante*: spectral density, mean direction, directional spreading, skewness and kurtosis (each for all 64 frequency bins), and 20 minute 1.28 Hz time series of buoy displacement in the vertical, north and west direction. The buoy was not equipped with an on-board data logger during FETCH, and since the ship was not always in the reception range, the time series and full spectral data are only available for about half of the time. The buoy sent also compressed directional spectra (13 spectral bands) via Argos satellite to cover the gaps.

[16] The buoy was moored using the standard double rubber cord mooring line. The natural frequency of this mooring line is 0.05 Hz, which is also, according to the manuals, the lowest reliable frequency. The highest measurable frequency is 0.6 Hz, defined by the dimensions of the buoy. The manufacturer, Datawell b.v., calibrated the buoy immediately after the experiment and all the calibrated parameters were within the specifications.

3. Directional Spectrum

[17] The traditional method to calculate the directional spectrum from buoys measuring three components of motion (either heave, pitch and roll or 3-accelerations) is that

presented by *Longuet-Higgins et al.* [1963]. The directional distribution is approximated with a Fourier series truncated to the first four coefficients that are possible to derive from the cross-spectrum. This is done routinely on board DWR. The mean direction, $\theta_1(f) = \arctan(b_1(f)/a_1(f))$, and the directional spreading $\sigma_1(f) = (2\,(1 - r_1(f)))^{1/2}$, where $r_1(f) = \sqrt{a_1(f)^2 + b_1(f)^2}$, are calculated from the first pair of Fourier coefficients:

$$a_1(f) = Q_{12}(f)/\sqrt{(C_{22}(f) + C_{33}(f))C_{11}(f)}$$

$$b_1(f) = Q_{13}(f)/\sqrt{(C_{22}(f) + C_{33}(f))C_{11}(f)},$$

where f is frequency and C_{ij} and Q_{ij} are the real and imaginary parts (co- and quad-) of the cross-spectrum between the ith and jth channels. Here, subscripts i and j can be either 1, 2 or 3, representing displacements in the vertical, north direction and west direction, respectively.

[18] To be able to compare the directional spectrum defined as above, the corresponding parameters were calculated from the two other wave sensors. In the case of the ASIS buoy, the local sea surface slopes (pitch and roll) were calculated from the wave staff array elevations. Then, $\theta_1(f)$ and $\sigma_1(f)$ were calculated as above where subscripts 1, 2 and 3 of C_{ij} and Q_{ij} now refer to displacement in the vertical direction, pitch angle and roll angle, respectively.

[19] RESSAC gives the two-dimensional wave number spectrum directly and the wave number spectrum has been converted to frequency spectrum, $F(f, \theta)$, using the dispersion relation for gravity waves in deep water. The co- and quad-spectra were calculated from this spectrum according to their definitions:

$$C_{11}(f) = \int_0^{2\pi} F(f,\theta)\,d\theta$$

$$C_{22}(f) = \int_0^{2\pi} k^2 F(f,\theta)\cos^2\theta\,d\theta$$

$$C_{33}(f) = \int_0^{2\pi} k^2 F(f,\theta)\sin^2\theta\,d\theta$$

$$C_{23}(f) = \int_0^{2\pi} k^2 F(f,\theta)\sin\theta\cos\theta\,d\theta$$

$$Q_{12}(f) = \int_0^{2\pi} kF(f,\theta)\cos\theta\,d\theta$$

$$Q_{13}(f) = \int_0^{2\pi} kF(f,\theta)\sin\theta\,d\theta,$$

where k is the measured wave number.

[20] The directional parameters $\theta_1(f)$ and $\sigma_1(f)$ do not contain enough information to solve the actual shape of the directional distribution [*Krogstad and Barstow*, 1999]. Another way to present the directional distribution is the two-dimensional spectrum, $F(f, \theta)$, itself. Direct comparison of $F(f, \theta)$ from different sensors is not a straightforward task, as pointed out by *Krogstad et al.* [1999]. Nevertheless, a two-dimensional spectrum reveals details of the directional distribution that cannot be obtained from the directional parameters. In this study the two-dimensional spectrum is used as a qualitative tool to interpret the environmental situation and differences between the wave sensors.

[21] To calculate the two-dimensional spectrum from the measurements of ASIS and DWR, the Maximum Likehood Method (MLM [*Capon*, 1969]) has been applied using the code by *Drennan et al.* [1994]. The two-dimensional spectra of the ASIS buoy have been calculated from the full set of 6 (5 in the first half of the experiment) wires and 28.5 min of data. In the case of DWR, the 20-min displacement time series were used.

[22] The number of frequency bins is for RESSAC 64 in the range 0.05–0.25 Hz, for ASIS 128 in the range 0.0078–1 Hz and for DWR 64 in the range 0.025–0.58 Hz. When the directional parameters derived from the cross-spectrum are used, the directional resolution is dependent not only on the degrees of freedom but also on the shape of the directional spectrum and it is not possible to give a definite directional resolution for the sensors [*Krogstad et al.*, 1999]. In the case of two-dimensional spectrum, the directional resolution of RESSAC is estimated to be 15°. For the MLM spectra the resolution is data dependent, and generally poorer than 15°.

4. Comparisons

4.1. ASIS–DWR Comparison

[23] First we compare the two moored buoys, ASIS and DWR, during the side-by-side intercomparison period from 19 March to 25 March at point B (Figure 1). The one-dimensional parameters, significant wave height, H_s, and peak frequency, $f_p = 1/T_p$ are plotted versus time in Figures 2c and 2d, respectively. The peak frequency is determined from the three frequencies that form the peak of the spectrum. The peak spreading angle and mean direction at the peak frequency are defined as mean of the values at the three frequencies that define the peak.

[24] Approximately 20% of the DWR data were received via Argos satellite alone. The Argos message consists of a 13-band spectrum and a significant wave height calculated on board the buoy. The peak frequency is the mean of the frequency band that forms the peak of the spectrum. The corresponding mean direction and directional spreading represent a mean value of this frequency band. Errors do randomly occur when data is transmitted via Argos but the reliability of the Argos data can be verified by repeated transmission. Most of the Argos spectra were received only once which makes these spectra somewhat uncertain. Hence these Argos data are not used in detailed (spectral) comparisons presented in the next section.

[25] In Figure 4a, H_s from the two buoys are plotted against each other as a scatterplot. Here, the DWR data have been interpolated onto the denser ASIS database to take account of time difference: the DWR values are calculated at half hourly intervals while those of ASIS are from every 28.5 min. The maximum likelihood regression (assuming equal variability [*Orear*, 1982]) is close to the 1:1 line,

$$H_{s,DWR} = 1.004H_{s,ASIS} + 0.033$$

and the correlation coefficient, γ^2, is 0.993. The coefficient of variation used in defining the 90% confidence limits due

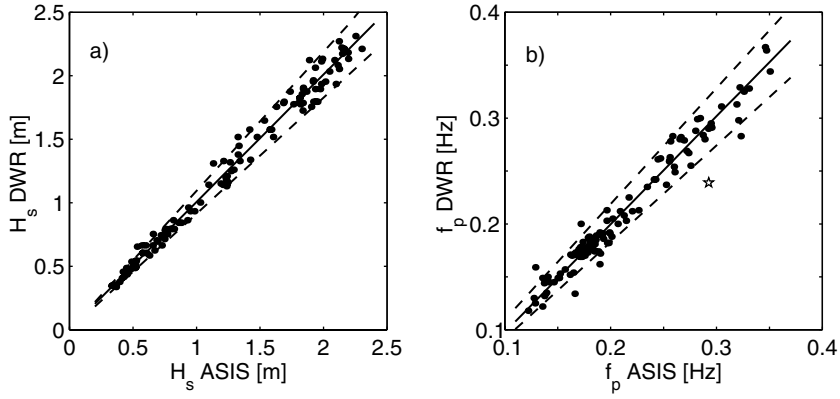

Figure 4. Comparison of significant wave height (a) and peak frequency (b) as measured by ASIS and DWR at location B. The solid lines are fits to the data and the dashed lines indicate the 90% confidence bands, assuming equal variability for the two sensors. The bimodal sea case, denoted by star in (b), has been excluded from the regression.

to sampling variability [*Allender et al.*, 1989; *Krogstad et al.*, 1999] was estimated from the data. The value of this coefficient, COV ≈ 0.05, is consistent with that reported by *Krogstad et al.* [1999] for a Directional Waverider deployed off Scotland. The 90% confidence limits are plotted in Figure 4a, and as 91% of the data points fall within these limits, the scatter in the plot can be attributed to sampling variability.

[26] The corresponding plot for peak frequency is shown in Figure 4b. The maximum likelihood regression line,

$$f_{p,DWR} = 1.021 f_{p,ASIS} - 0.004$$

($\gamma^2 = 0.981$), shows no significant difference between the two estimates. Again, over 90% of the points fall within the 90% confidence limits. The single point (denoted by star in Figure 4b) that differs clearly from the regression line is associated with a bimodal sea state with the two spectral modes containing comparable energies. In this case the two buoys select different modes as the peak of the spectrum and therefore the point is excluded from the regression.

[27] Next we compare the directional parameters. Figure 2e shows the time series of the spreading angles σ_p at the peak frequency. Most of the time the agreement is good, but there are some times (mostly between 22 March 1200 and 23 March 2400) where the spreading values reported by DWR are much smaller. In Figure 5a the spreading angles at the peak frequency are plotted against each other. Excluding this period around 23 March (denoted by in Figure 5a), the agreement is generally good, with $\gamma^2 = 0.87$. On average, the DWR peak spreading angles are 3° narrower than those of ASIS. Around 23 March, a period dominated by light-moderate winds and swell, the agreement in σ_p is poor, with ASIS showing significantly higher spreading.

[28] The spreading angles are scattered more evenly if we consider all frequencies above the peak, $f \geq f_p$, and with

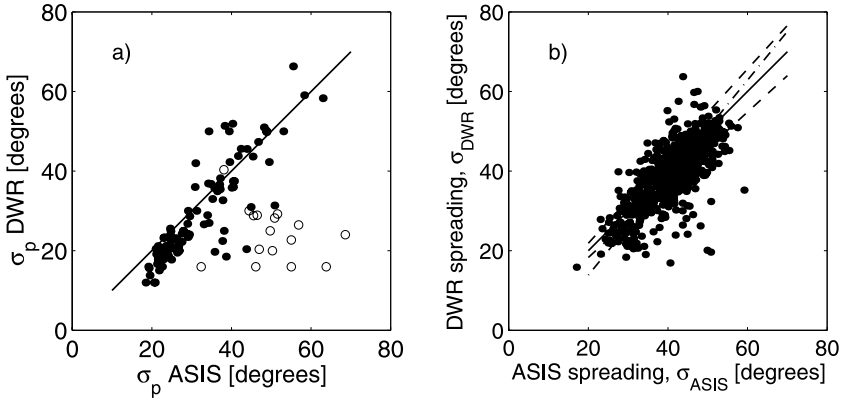

Figure 5. Comparison of directional spreading, σ_1, calculated following *Longuet-Higgins et al.* [1963], for ASIS and DWR at location B. Panel a): spreading at the peak frequency. Data from 22 March, 1200 UTC, to 23 March, 2400 UTC, indicated by . Panel b): σ_1, at all frequencies above the peak, and with energy $E > 0.02\ E_{max}$. The dashed lines indicate the 90% confidence bands, assuming equal variability for the two sensors. The dashed-dotted line is a fit to the data and the solid line the 1:1 relationship.

energy levels above 0.02 $E_{\max}$ (Figure 5b). However, the maximum likelihood regression line

$$\sigma_{1,DWR} = 1.2\sigma_{1,ASIS} - 10.6,$$

($\gamma^2 = 0.74$) is significantly different from the 1:1 line. Again, the largest differences occur around 23 March. Note that the data sets making up panels a) and b) are different. The plot of σ_p includes DWR summary data (peak parameters) transmitted by Argos; only cases where the frequency-dependent information is available are used in panel b).

[29] It is unclear why the data from 23 March are distinct from the remainder of the period. In a comparison of DWR and ASIS σ_1 (f) during this period (not shown), it is evident that the largest disagreements occur near the spectral peak; at higher frequencies, the buoys usually report similar values of σ_1. An exception to this occurs late on 23 March, when the winds turn from S to NE over a couple of hours. During this interval, ASIS σ_1 are uniformly broad. This is due to the slow rotation of the ASIS buoy during turning winds.

[30] In its tethered configuration, the orientation of ASIS with respect to its tether buoy is determined by a combination of wind and surface current forcing. During FETCH, surface currents were weak, so that wind forcing was the dominant factor except at very light winds. Consequently, the buoy orientation or heading is aligned in the wind direction. If the wind direction changes significantly during a run, the buoy heading will also change. Since the ASIS data processing is carried out in 28.5 min blocks (assumed to be stationary) such a heading change within a block will produce a increase in the measured wave spreading. In these nonstationary conditions, a method such as the wavelet directional method [*Donelan et al.*, 1996], which uses the instantaneous heading, should be used to process the data.

[31] The last parameter to compare, the mean direction at the peak, θ_p, is plotted as a function of time in Figure 2b. In general, the buoys agree quite well with a mean difference of 5.8°.

4.2. ASIS–DWR–RESSAC Comparison

[32] Due to the fact that RESSAC spectra are reliable only for $H_s > 1$ m, the seven Merlin-IV flights yielded four cases for detailed comparison. Basic parameters from these RESSAC measurements are shown in Figures 2 and 3. The four cases are studied individually. When comparing mean directions, the 180° ambiguity in the RESSAC directions has been removed on the basis of the directions reported by the two other wave sensors. The ambiguity has been retained in the RESSAC two-dimensional spectra. The results concerning the significant wave height have been verified by calculating H_s for the moored buoys using the high frequency limit of RESSAC, 0.25 Hz.

4.2.1. 20 March: Three Different Meteorological Events

[33] The meteorology on 20 March was dominated by a Mistral that started on the previous evening. Around the middle of the day (20 March), there was a temporary weakening of the wind. The high winds resumed during the evening, with the wind speed growing rapidly to 15 ms^{-1} a few hours before the RESSAC observations. At that time wind was steady but fetch limited conditions had not yet been reached (Figure 2).

[34] Three events during the day are selected for comparison. The first event is at the peak of the Mistral at 0100 UTC. The one-dimensional spectra and parameters of ASIS and DWR plotted in Figure 6a show that the agreement is good. This is also the case in the second event at 1030 UTC when the wind was weakening (Figure 6b). During the third event, at the time of the RESSAC observations at 2200 UTC, there were no coincident DWR measurements. The one-dimensional spectra and parameters reported by RESSAC and ASIS are consistent (Figure 6c). In all the cases the directional parameters (Figure 6, middle and lowest panels) also agree well, with a small offset in the mean directions (Figure 6, middle panels). The two-dimensional spectra of ASIS and RESSAC at 2200 UTC have similar shapes (Figure 7). The broader distribution of the ASIS spectrum can be attributed to the MLM analysis which typically gives a rather broad spectrum [e.g., *Donelan et al.*, 1996; *Ewans*, 1998]: the spreading parameter does not show much difference between the two sensors (Figure 6c, lowest panel).

4.2.2. 24 March: A Fetch-limited Case

[35] On 24 March, the experimental region was under the influence of a second Mistral event with northerly winds up to 18 ms^{-1} (Figures 2a–2b). We focus on the period around 1740 UTC when data are available from both RESSAC and ASIS. Although no DWR data are available at that time, there is a full DWR spectrum from two hours earlier (1530 UTC). The wave growth for this period was fetch limited, and from 1030 to 1800 UTC the wind as measured at ASIS fulfills the requirements for steady wind conditions when data are used in fetch limited growth analysis [cf. *Kahma and Calkoen*, 1992, Figure 12a]. At the mean wind speed of 13 ms^{-1}, waves require 5 hours to grow from shore to the 60 km fetch. Therefore by 1530 UTC the wave field can be considered as steady at the mooring site. This was verified using the ASIS data. Consequently, we combine the 1530 DWR data with the 1740 RESSAC and ASIS data for the comparison.

[36] The one-dimensional spectra from the three wave sensors are plotted in Figure 8a. The shape of the spectra agree well, as do the basic parameters. The mean direction and spreading, plotted as a function of frequency in Figures 8b and 8c, are in agreement in the energy containing regions for three wave sensors. Here, like in the two cases on 20 March (Figures 6a–6b, lowest panels and Figure 8c), the spreading curves of DWR show a sudden drop at lower frequencies. We believe this behavior is an artifact related to the mooring of DWR. It can occasionally be observed in cases when there is no detectable energy at these frequencies [*Drennan et al.*, 2003b].

[37] The two-dimensional spectra are plotted in Figure 9. It is evident that the RESSAC spectrum shows more detail than the buoy MLM spectra. For instance, the RESSAC spectrum shows two wave modes near the peak frequency while ASIS and DWR each have broad single mode. The continued presence of the bimodal sea along

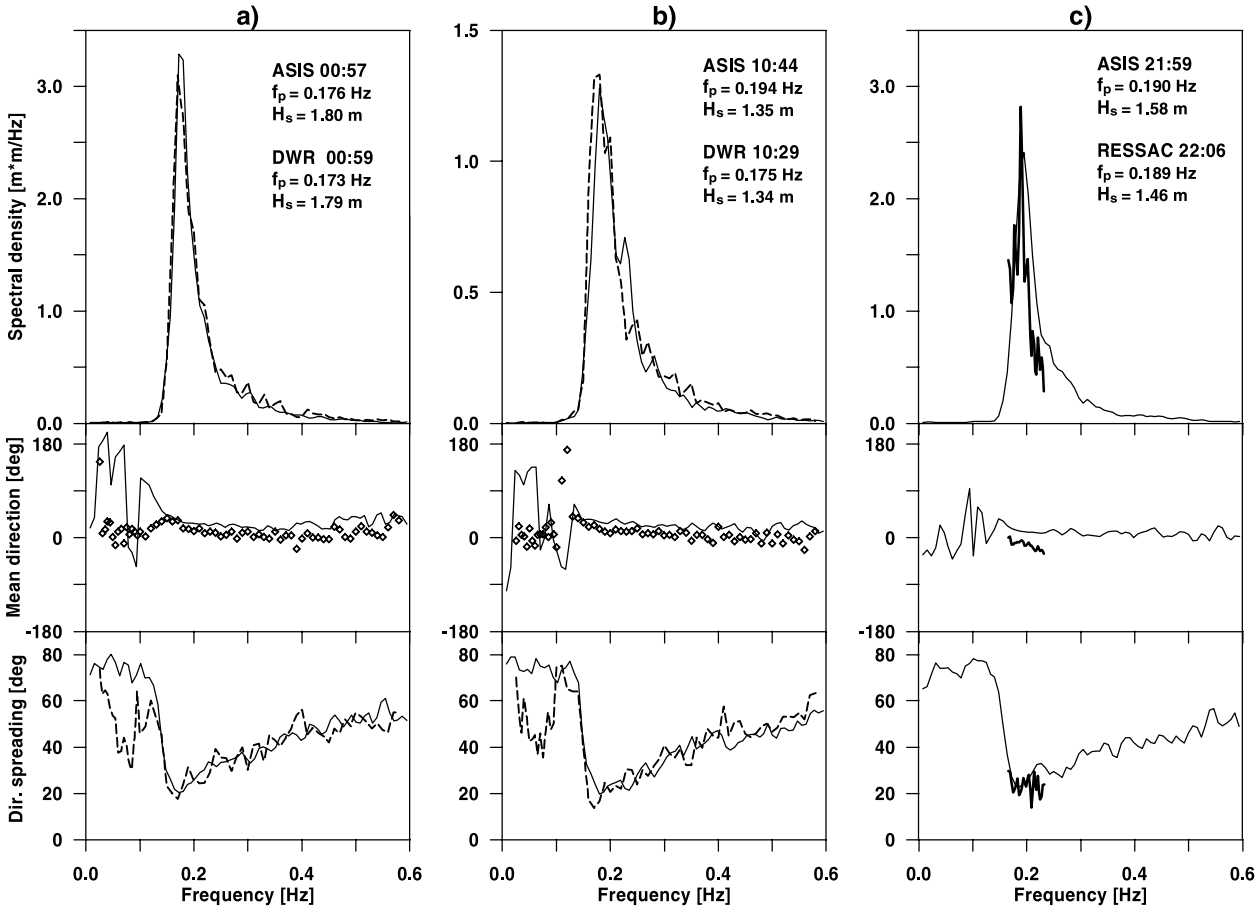

Figure 6. Case of 20 March: one-dimensional spectra, mean direction (arriving from) and directional spreading as a function of frequency. Panel a: ASIS (line) and DWR (dashed line and ◇) at 0100 UTC, location B. Panel b: ASIS (line) at 1044 UTC and DWR (dashed line and ◇) at 1030 UTC, location B. Panel c: ASIS (medium line) at 2159 UTC, location B and RESSAC (thick line) at 2206 UTC, near location B (43.00°N, 4.27°E).

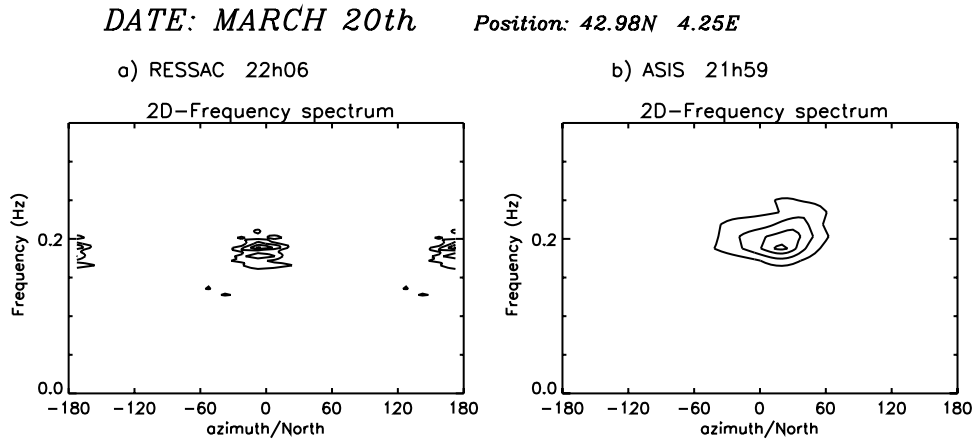

Figure 7. Case of 20 March: two-dimensional spectra obtained from RESSAC and ASIS. Panel a: RESSAC at 2206 UTC near location B (43.00°N, 4.27°E). Panel b: ASIS at 2159 UTC at location B. The normalized energy density (with respect to the peak) is plotted with contour levels of 0.25, 0.50, 0.75, and 0.95. The horizontal axis gives the azimuth (from true north), the vertical axis is for the frequency (Hz). For ASIS, the directions refer to waves arriving from. For RESSAC, the 180° ambiguity in direction has not been removed and only frequencies higher than 0.123 Hz are considered for the plot.

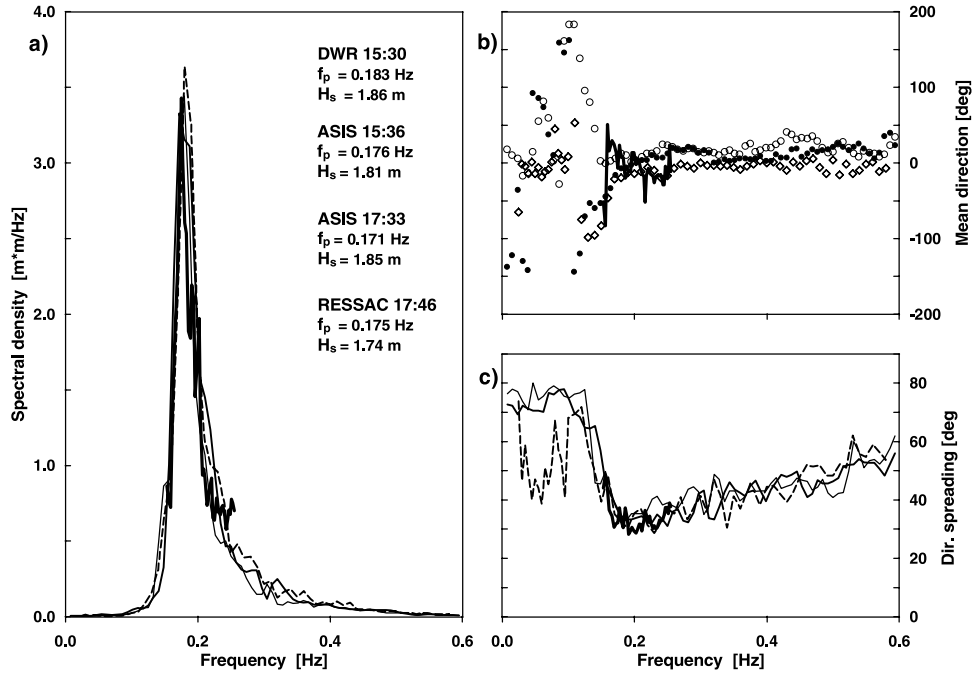

Figure 8. Case of 24 March: panel a: one-dimensional spectra, panel b: mean direction (arriving from) and panel c: directional spreading. RESSAC (thick line) at 1746 UTC and ASIS (medium line and ○) at 1733 UTC. ASIS (thin line and ●) at 1536 UTC and DWR (dashed line and ◇) at 1530 UTC. ASIS and DWR are at location B, RESSAC near location B at 43.02°N, 4.24°E.

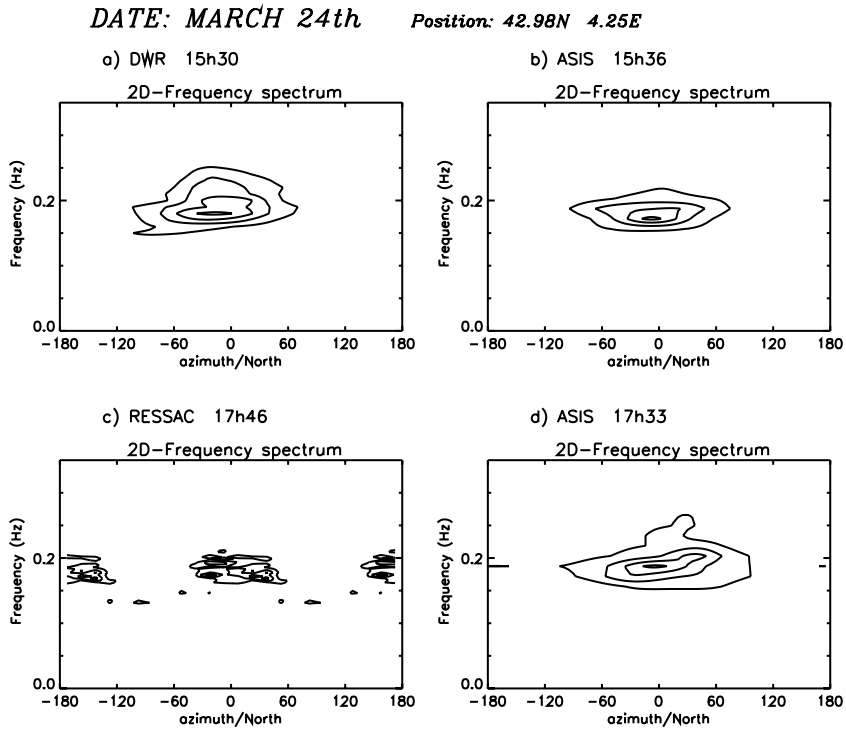

Figure 9. Case of 24 March: two-dimensional spectra obtained from DWR, ASIS and RESSAC. Panel a: DWR at location B at 1530 UTC. Panel b: ASIS at location B at 1536 UTC, Panel c: RESSAC near location B (43.02°N, 4.24°E) at 1746 UTC. Panel d: ASIS at location B at 1733 UTC. Conventions for contours are the same as in Figure 7, except that for RESSAC the minimum frequency considered in the plot is 0.127 Hz.

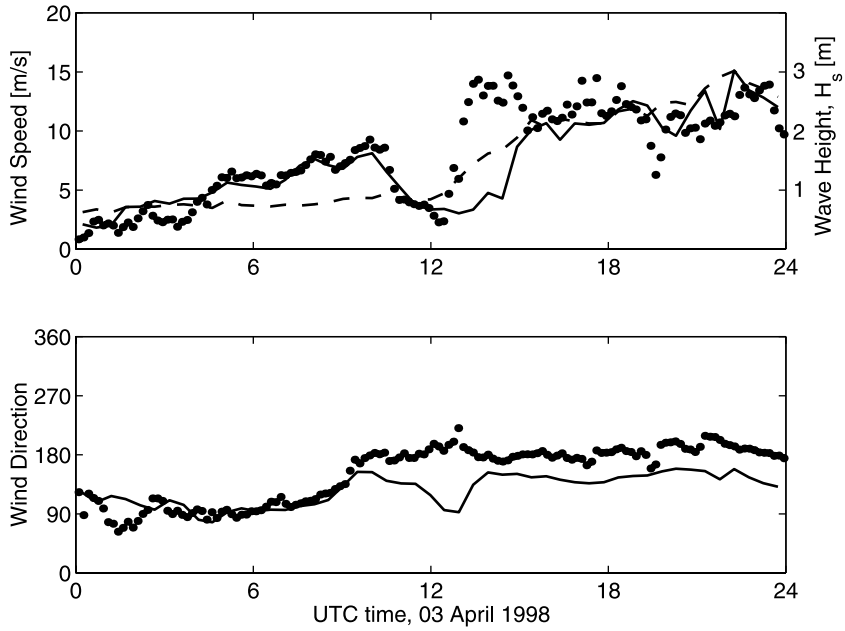

Figure 10. The wind speed and direction from ASIS (line) and R/V *l'Atalante* (●) on 3 April. During most of the day, R/V *l'Atalante* maintained a steady course into the wind, passing ASIS around 0900 UTC. By 1300 UTC, the two platforms were roughly 40 km apart. The dashed line is the significant wave height H_s reported by ASIS.

the RESSAC flight track indicates that this is real feature, one that is clearly absent from the buoy spectra. The origin of the two modes can be found in the specific wind field pattern and the shape of the coast. On 24 March the Mistral formed a belt of high winds which narrowed toward south. Close to the shore the wind directions were nearly orthogonal to the curved shore line. The horizontal distribution of the wind directions together with the differences in fetch along the shoreline resulted in the bimodal or broad spectra reported by the sensors. Given that two wave modes are at the same frequency, and separated by less than 50 degrees in direction, it is likely this is beyond the resolution of the maximum likelihood method used to derive the two-dimensional buoy spectra. We note that the three sensors agree in spreading width at this frequency: only the two-dimensional representation shows some differences.

4.2.3. 3 April: An Inhomogeneous Wind Field

[38] During the second part of the experiment DWR was moored closer to the shore, at point B′ in Figure 1. On 3 April, the surface wind in the western Mediterranean Sea, as determined by the atmospheric model Aladin, was strongly inhomogeneous with sharp gradients and a 100 km scale cyclonic circulation. According to the wind measurements at ASIS and R/V *l'Atalante* this circulation generated 10–14 ms^{-1} south–southeast winds in the experimental area during the RESSAC flight in the afternoon. At the position of R/V *l'Atalante* offshore of the buoys (see Figure 1) the wind rose from 3 ms^{-1} to 14 ms^{-1} between 1230 and 1330 UTC (Figure 10). At the ASIS position, a mere 40 km north–northwest from R/V *l'Atalante*, this increase occurred 1.7 hours later, an expression of the inhomogeneity of the wind field.

[39] The one-dimensional spectra and directional parameters for the pairs RESSAC/DWR and RESSAC/ASIS are plotted in Figures 11 and 12 respectively, and the two-dimensional spectra in Figure 13. Closer to the shore, DWR at 1630 UTC reports a swell from the south and shorter waves from the southeast (Figure 11 and panels e and f in Figure 13). The RESSAC observations are in agreement with those of DWR (Figure 11 and panel d in Figure 13). The energy levels at higher frequencies were on the limit of RESSAC's operational range causing scatter in corresponding mean directions (Figure 11b).

[40] Southeast of the position of DWR, at 1622 UTC, ASIS and RESSAC agree on the one-dimensional spectrum with a 10 cm difference in the significant wave height (Figure 12a). In the hours preceding this, the wave field at ASIS was rapidly evolving (compare the ASIS data from 1425 UTC and 1622 UTC in Figure 12). In Figure 10, it is evident that the wave height at ASIS starts to increase by 1230 UTC, several hours before the wind speed. This growth of the wave field at ASIS is too rapid to be accounted for by local production [*Kahma and Calkoen*, 1992]. On the basis of the ASIS spectra from 1300–1600 UTC (not shown), the additional wave energy has been advected into the region from the south-southeast, where the front passed earlier. With a constant frontal propagation speed of 6.3 ms^{-1} (estimated from Figure 10), the 14 ms^{-1} southeast winds behind the front would have arrived about 70 km south-southeast of ASIS by 9 to 10 UTC. Using the group velocity 5.7 ms^{-1} to estimate the wave energy propagation speeds, wind waves created in this region would have reached the ASIS position by the time of the ASIS measurements.

[41] ASIS and RESSAC report the directional parameters consistently, though the mean direction has again a small

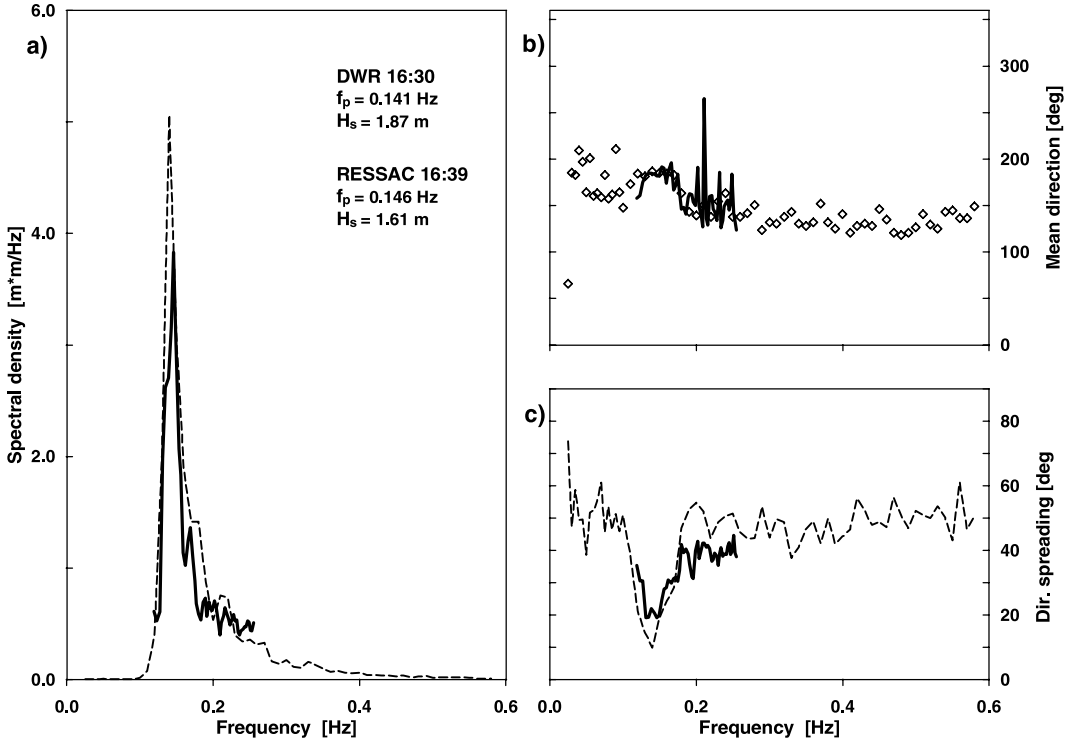

Figure 11. Case of 3 April: panel a: one-dimensional spectra, b: mean direction (arriving from) and panel c: directional spreading. DWR (dashed line and ◇) at 1630 UTC, location B′ and RESSAC (thick line) at 1639 UTC, location near B′ (43.19°N, 4.11°E).

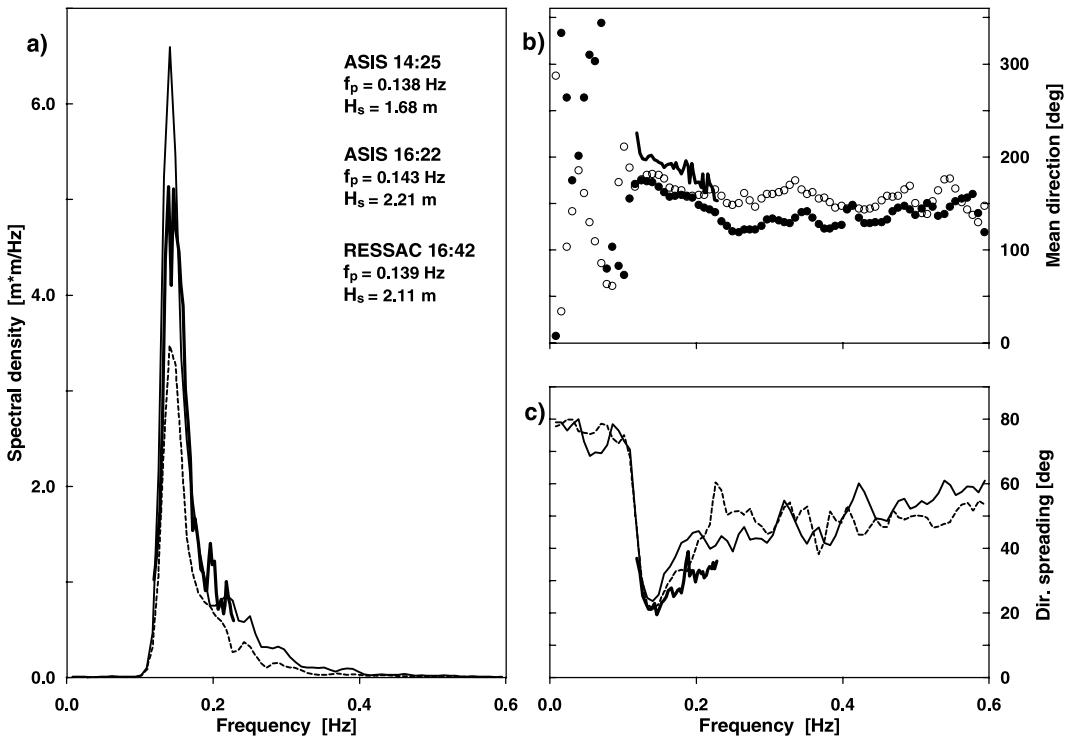

Figure 12. Case of 3 April: panel a: one-dimensional spectra, b: mean direction (arriving from) and panel c: directional spreading. ASIS (line and ○) at 1622 UTC, location B and RESSAC (thick line) at 1642 UTC, location near B (43.00°N, 4.27°E) and ASIS (dashed line and ●) at 1425 UTC, location B.

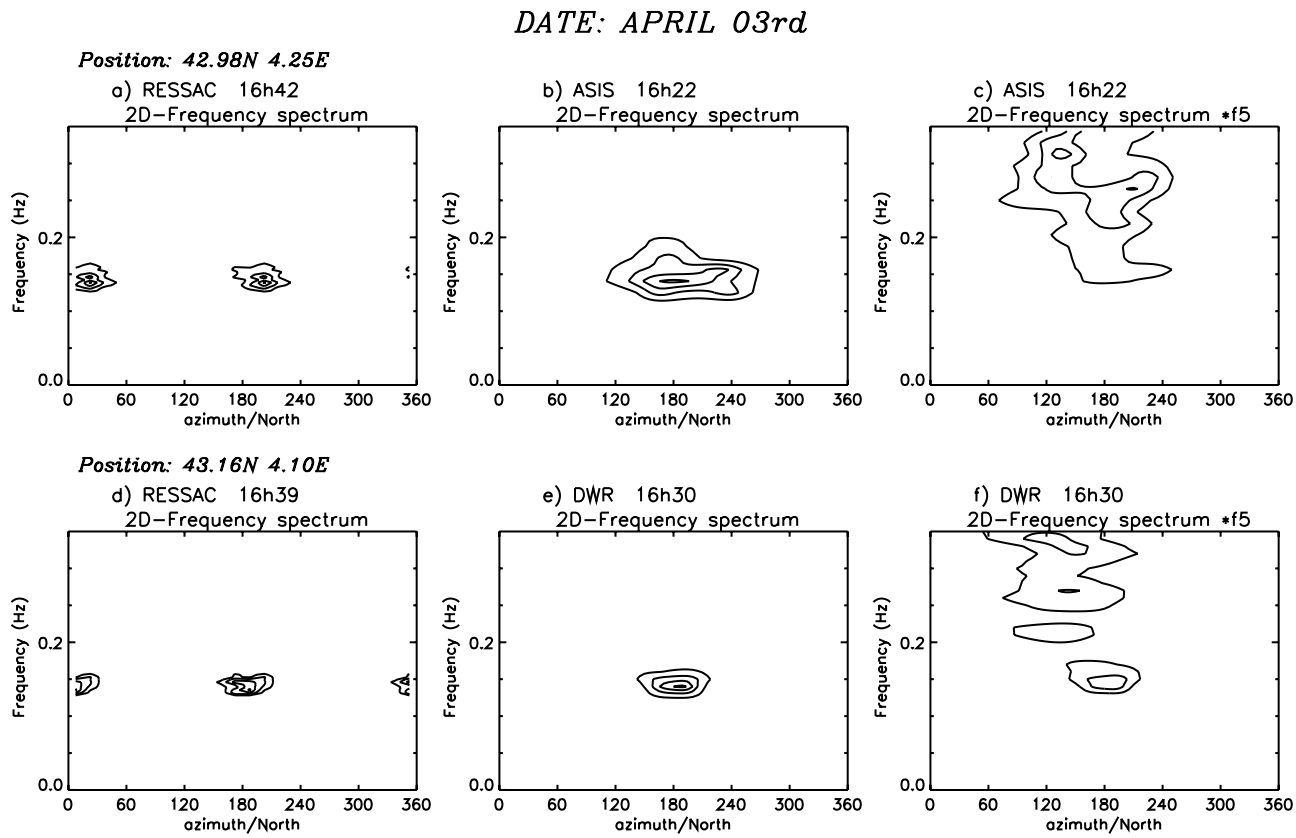

Figure 13. Case of 3 April: two-dimensional spectra obtained from RESSAC, ASIS and DWR. Panel a: RESSAC at 1642 UTC near location B (43.00°N, 4.27°E). Panel b: ASIS at 1622 UTC at location B. Panel c: Same as b, but for the spectrum multiplied by f^5. Panel d: RESSAC at 1639 UTC near location B′ (43.19°N, 4.11°E). Panel e: DWR at 1630 UTC at location B′. Panel f: same as e, but for the spectrum multiplied by f^5. Conventions for contours are the same as in Figure 7, except that for RESSAC the minimum frequency considered in the plot is 0.090 Hz.

offset (Figure 12b) and RESSAC reports a slightly narrower distribution above the peak (Figure 12c). The two-dimensional spectrum of RESSAC at 1642 UTC shows a narrow swell from 200° (Figure 13a), while the two-dimensional ASIS spectrum is broader with a mean direction of 180° at the spectral peak (Figure 13b). The RESSAC spectrum multiplied by f^5 shows, in the limits of the operational range, southeastern waves at higher frequencies (not shown) in agreement with ASIS which also reports wind waves from around 140° (Figure 13c). The RESSAC spectra along the flight track (see the trajectory in Figure 1) show that from the position of DWR toward the open sea the wave spectrum becomes broader (Figure 14). This is consistent with the buoy observations: ASIS, further offshore, reports a broader spectrum than DWR (Figures 13b and 13e or Figures 11c and 12c). The spatial evolution of the spectrum may contribute to the observed difference between the RESSAC and ASIS two-dimensional spectra (panels a and b in Figure 13), but, like in the two previous cases, also the tendency of MLM to broaden the spectrum can be part of the reason for the difference.

[42] In this strongly inhomogeneous situation the three sensors show good degree of consistency, but we cannot rule out the possibility that the basic assumptions of spectrum analysis, stationarity in the case of ASIS and homogeneity in the case of RESSAC, have been violated too much.

[43] This case demonstrates the complementary nature of the buoy and airborne sensors. The buoys provide the evolution of the wave field as a function of time (e.g., H_s in Figure 10), whereas the radar provides the evolution of the wave field in space (Figure 14). In complicated meteorological situations such as this, the availability of data from both types of sensor greatly facilitates an understanding of the wave field.

4.2.4. 7 April: A Swell Case

[44] The last case, on 7 April, shows the wave field after a passage of an atmospheric frontal discontinuity, a frequently encountered situation during the second part of the experiment. Before the passage, the wind was from the south–southeast with wind speeds over 10 ms^{-1}. After the frontal passage the wind turned to northwest, decreasing to 4 ms^{-1} (Figure 3). At the ASIS location the significant wave height was on the limit of RESSAC's operational range as can be seen in the one-dimensional spectrum close to ASIS (Figure 15a). The two-dimensional spectrum of ASIS (Figure 15c) shows two wave fields, one from the

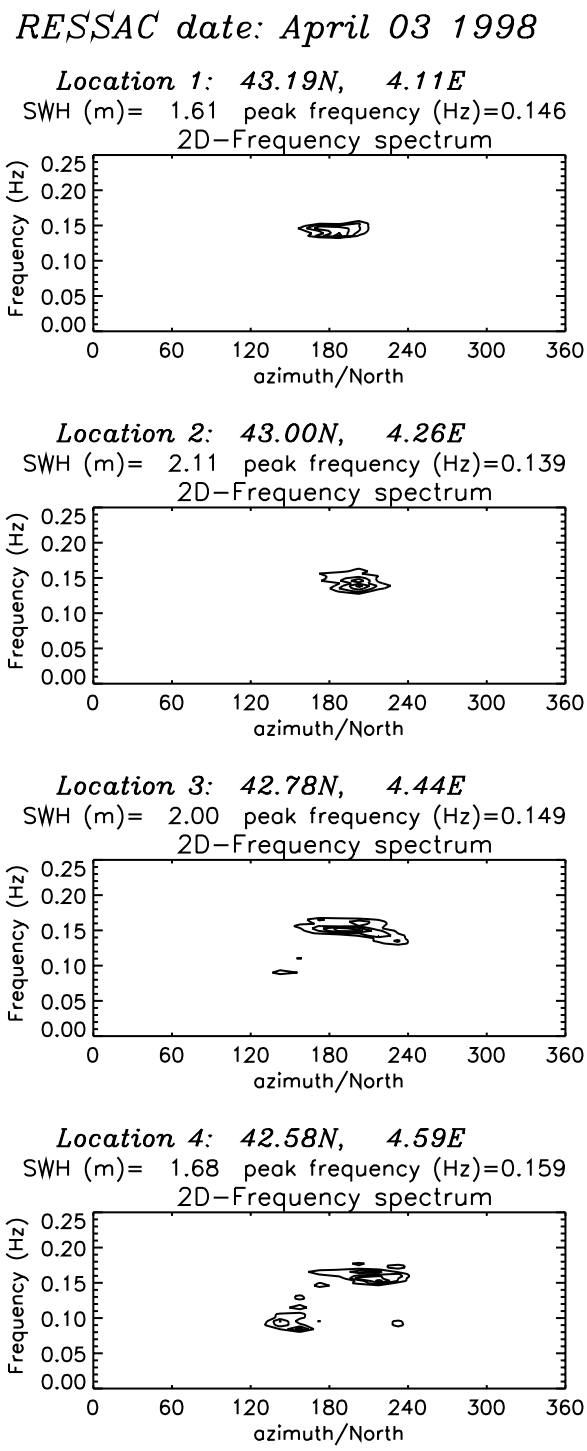

Figure 14. Case of 3 April: two-dimensional RESSAC spectra at four different locations along the flight track in Figure 1, from north to south. The ambiguity has been removed for clarity. The panel at the top: near the location of DWR at B′ (43.19°N, 4.11°E). Second panel: near the location of ASIS at B (43.00°N, 4.27°E). Third panel: at location 42.72°N, 4.44°E. The lowest panel: at location 42.58°N, 4.59°E. Conventions for contours are the same as in Figure 7, except that for RESSAC the minimum frequencies considered in the panels are from top to bottom 0.135 Hz, 0.115 Hz, 0.090 Hz and 0.071 Hz.

south at lower frequencies and one from west–southwest at higher frequencies. The wave field reported by RESSAC has the same features (Figure 15b). In spite of the limited performance of RESSAC in this case, both ASIS and RESSAC report a clear case of a mixed sea with local wind waves and swell whose directions at the peak frequencies are separated by about 60 degrees. On this flight the track of RESSAC did not go over the position of the DWR, but the buoy reported a wave field that is consistent with the other wave sensors. As the energy levels were low, the comparisons of the mean direction and spreading have not been made.

5. Conclusions

[45] The performance of three wave sensors with different measuring principles was studied in a variety of meteorological conditions during the FETCH experiment. Two of the wave sensors were moored buoys, an Air–Sea Interaction Spar buoy ASIS and a Directional Waverider DWR. The third was an airborne radar, RESSAC. In the limits of their operational ranges, the sensors reported the one-dimensional spectrum and the basic parameters, the significant wave height and spectral peak frequency, consistently.

[46] Directional properties of a wave field are more problematic to measure and quantify. In addition to instrumental limitations, different analysis techniques are not necessarily consistent. In this study mean direction and directional spreading as defined by *Longuet-Higgins et al.* [1963] were used. The spreading parameter, based on the first pair of the Fourier coefficients, is unable to describe the actual shape of the directional distribution [*Krogstad and Barstow*, 1999] but it is still an indicator of the directional width of the spectrum. Using the spreading parameter the higher directional resolution of RESSAC and ASIS was not taken into account.

[47] The two-dimensional spectra of the three sensors were qualitatively studied. In the cases studied in detail, the sensors reported the shape of the two-dimensional spectrum consistently. Only in a strongly inhomogeneous situation were some small differences between ASIS and RESSAC found. The two-dimensional spectra of RESSAC, which provides a more direct measurement, showed in most cases more details than the two-dimensional spectra of ASIS and DWR. Although the directional spreading of buoy and radar observations are generally in good agreement, the two-dimensional spectra obtained from the buoy data with MLM are typically broader than radar two-dimensional spectra. This shows that when combining different sensors, the directional spreading parameter must be calculated in a consistent way, i.e., from the co- and quad- spectra. Spreading values obtained from retrieved two-dimensional spectra should not be used, as they are dependent not only on the input data, but also on the analysis method (e.g., MLM).

[48] Measuring the directional properties of a wave field is a difficult task, especially when the directional width of the spectrum is studied. Also, this study showed that there can occasionally be significant differences between wave sensors and combining or comparing results from different wave sensors cannot be done reliably if the performance of

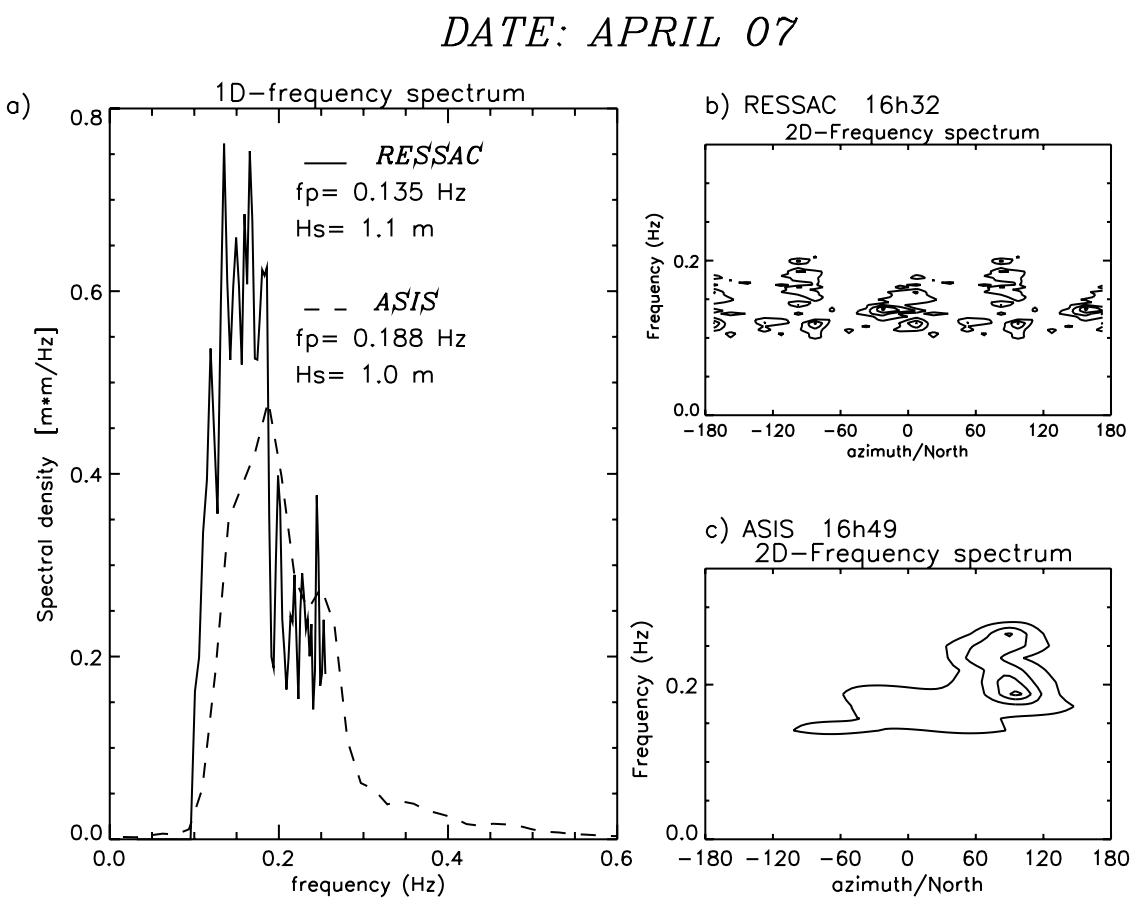

Figure 15. Case of April 7: panel a: one-dimensional spectrum of RESSAC (solid line), and ASIS (dashed line). Panel b: two-dimensional spectrum of RESSAC at 1632 UTC and at location 43.03°N, 4.38°E. Panel c: two-dimensional spectrum of ASIS at 1649 UTC at point B. Conventions for contours are the same as in Figure 7, except that for RESSAC the minimum frequency considered in the plot is 0.096 Hz.

the sensors themselves with respect to each other is not known.

[49] **Acknowledgments.** We thank the following people who contributed to the success of this work: H. Dupuis (DGO-Bordeaux), L. Eymard (CETP), J. Gabriele (NWRI, Canada), M. Rebozo (RSMAS), and H. Söderman (FIMR), as well as the officers and crew of R/V *l'Atalante*. In addition, we gratefully acknowledge support for the FETCH experiment from the European Community MAST programme, grant CEE MAS3.CT96.0051, and from the French "Institut National des Sciences de l'Univers" (PATOM and PNTS grants).

References

Allender, J., T. Audunson, S. F. Barstow, S. Bjerken, H. E. Krogstad, P. Steinbakke, L. Vardel, and L. E. Borgman, The WADIC project: A comprehensive field evaluation of directional wave instrumentation, *Ocean Eng.*, *16*, 505–536, 1989.

Beal, R. C., (Ed.), *Directional Ocean Wave Spectra*, 218 pp., Johns Hopkins Univ. Press, Baltimore, 1991.

Capon, J., High-resolution frequency-wavenumber spectrum analysis, *Proc. IEEE*, *57*, 1408–1418, 1969.

Donelan, M. A., W. M. Drennan, and A. K. Magnusson, Non-stationary analysis of the directional properties of propagating waves, *J. Phys. Oceanogr.*, *26*, 1901–1914, 1996.

Drennan, W. M., M. A. Donelan, N. Madsen, K. B. Katsaros, E. A. Terray, and C. N. Flagg, Directional wave spectra from a Swath ship at sea, *J. Atmos. Oceanic Technol.*, *11*, 1109–1116, 1994.

Drennan, W. M., H. C. Graber, M. A. Donelan, and E. A. Terray, Directional wave measurements from the ASIS (air–sea interaction spar) buoy, *Proc. Oceans*, *98*, 414–418, 1998.

Drennan, W. M., H. C. Graber, D. Hauser, and C. Quentin, On the wave age dependence of wind stress over pure wind seas, *J. Geophys. Res.*, *108*, doi:10.1029/2000JC000715, in press, 2003a.

Drennan, W. M., K. K. Kahma, H. C. Graber, H. Pettersson, M. A. Donelan, and D. Hauser, ASIS-Directional Waverider comparison, in *Measuring and Analysing the Directional Spectrum of Ocean Waves*, edited by Action COST714 WG3, Eur. Comm., in press, 2003b.

Dupuis, H., C. Guérin, D. Hauser, A. Weill, P. Nacass, W. M. Drennan, S. Cloché, and H. C. Graber, Impact of flow distortion corrections on turbulent fluxes estimated by the inertial dissipation method during the FETCH experiment on R/V L'Atalante, *J. Geophys. Res.*, *108*, doi:10.1029/2001JC001075, in press, 2003.

Ewans, K. C., Observations of the directional spectrum of fetch-limited waves, *J. Phys. Oceanogr.*, *28*, 495–512, 1998.

Graber, H. C., E. A. Terray, M. A. Donelan, W. M. Drennan, J. Van Leer, and D. B. Peters, ASIS—A new air–sea interaction spar buoy: Design and performance at sea, *J. Atmos. Oceanic Technol.*, *17*, 708–720, 2000.

Hauser, D., G. Caudal, G. J. Rijckenberg, D. Vidal-Madjar, G. Laurent, and P. Lancelin, RESSAC: A new air-borne FM/CW radar ocean wave spectrometer, *IEEE Trans. Geosci. Remote Sens.*, *30*, 981–995, 1992.

Hauser, D., et al., The FETCH experiment: An overview, *J. Geophys. Res.*, *108*(C3), 8053, doi:10.1029/2001JC001202, 2003.

Jackson, F. C., and W. T. Walton, A comparison of in situ and airborne radar observations of ocean wave directionality, *J. Geophys. Res.*, *90*, 1005–1018, 1985.

Jackson, F. C., W. T. Walton, and P. L. Baker, Aircraft and satellite measurement of ocean wave directional spectra using scanning-beam mircowave radars, *J. Geophys. Res.*, *90*, 987–1004, 1985.

Kahma, K. K., and C. C. Calkoen, Reconciling discrepancies in the observed growth of wind-generated waves, *J. Phys. Oceanogr.*, *22*, 1389–1405, 1992.

Krogstad, H. E., and S. F. Barstow, Directional distributions in ocean wave spectra, in *Proceedings of the Ninth International Offshore and Polar Eng. Conference, Brest, France, May 30–June 4 1999*, pp. 79–86, 1999.

Krogstad, H. E., J. Wolf, S. P. Thompson, and L. R. Wyatt, Methods for intercomparison of wave measurements, *Coastal Eng.*, *37*, 235–257, 1999.

Longuet-Higgins, M. S., D. E. Cartwright, and N. D. Smith, Observations of the directional spectrum of sea waves using the motion of a floating buoy, in *Ocean Wave Spectra: Proceedings of a Conference*, pp. 111–132, Prentice-Hall, Old Tappan, N.J., 1963.

Orear, J., Least squares when both variables have uncertainties, *Am. J. Phys.*, *50*, 912–916, 1982.

O'Reilly, W. C., T. H. C. Herbers, R. J. Seymour, and R. T. Guza, A comparison of directional buoy and fixed platform measurements of Pacific swell, *J. Atmos. Oceanic Technol.*, *13*, 231–238, 1996.

Quentin, C., and D. Hauser, Directional wave spectra during FETCH from the airborne radar RESSAC, *Réunion bilan, présentations des premiers résultats, Doc. FETCH No. 11*, pp. 37–63, Cent. Etud. des Environ. Terr. et Planét., Vélizy, France, 1999.

Wyatt, L. R., S. P. Thompson, and R. R. Burton, Evaluation of high frequency radar wave measurement, *Coastal Eng.*, *37*, 259–282, 1999.

M. A. Donelan, W. M. Drennan, and H. C. Graber, Rosenstiel School of Marine and Atmospheric Science, University of Miami, 4600 Rickenbacker Causeway, Miami, FL 33149, USA. (mdonelan@rsmas.miami.edu; wdrennan@rsmas.miami.edu; hgraber@rsmas.miami.edu)

D. Hauser and C. Quentin, Centre d'Etude des Environnements Terrestres et Planétaires (CETP), 10–12 Avenue de l'Europe, F-78140, Vélizy, France. (daniele.hauser@cetp.ipsl.fr; celine.quentin@cetp.ipsl.fr)

K. K. Kahma and H. Pettersson, Finnish Institute of Marine Research, P.O. Box 33, FIN-00931, Helsinki, Finland. (kimmo.kahma@fimr.fi; heidi.pettersson@fimr.fi)